

Observation of a long-range unidirectional charge density wave in kagome superconductor KV_3Sb_5

Xingwei Shi(石兴伟), Xiao Liu(刘潇), Geng Li(李更), Zhen Zhao(赵振), Haitao Yang(杨海涛), Xiao Lin(林晓), and Hong-Jun Gao(高鸿钧)

Citation: Chin. Phys. B, 2025, 34 (**7**): 077101. DOI: 10.1088/1674-1056/add7ad
http://cpb.iphy.ac.cn; http://iopscience.iop.org/cpb

What follows is a list of articles you may be interested in

The de Haas-van Alphen quantum oscillations in the kagome metal $RbTi_3Bi_5$

Zixian Dong(董自仙), Lei Shi(石磊), Bin Wang(王彬), Mengwu Huo(霍梦五), Xing Huang(黄星), Chaoxin Huang(黄潮欣), Peiyue Ma(马培跃), Yunwei Zhang(张云蔚), Bing Shen(沈冰), and Meng Wang(王猛)
Chin. Phys. B, 2024, 33 (**10**): 107102. DOI: 10.1088/1674-1056/ad6a0a

In-plane uniaxial-strain tuning of superconductivity and charge-density wave in CsV_3Sb_5

Xiaoran Yang(杨晓冉), Qi Tang(唐绮), Qiuyun Zhou(周秋韵), Huaiping Wang(王怀平), Yi Li(李意), Xue Fu(付雪), Jiawen Zhang(张加文), Yu Song(宋宇), Huiqiu Yuan(袁辉球), Pengcheng Dai(戴鹏程), and Xingye Lu(鲁兴业)
Chin. Phys. B, 2023, 32 (**12**): 127101. DOI: 10.1088/1674-1056/acf707

Electronic states of domain walls in commensurate charge density wave ground state and mosaic phase in 1*T*-TaS_2

Yan Li(李彦), Yao Xiao(肖遥), Qi Zheng(郑琦), Xiao Lin(林晓), Li Huang(黄立), and Hong-Jun Gao(高鸿钧)
Chin. Phys. B, 2023, 32 (**7**): 077101. DOI: 10.1088/1674-1056/accd4f

Flat band in hole-doped transition metal dichalcogenide observed by angle-resolved photoemission spectroscopy

Zilu Wang(王子禄), Haoyu Dong(董皓宇), Weichang Zhou(周伟昌), Zhihai Cheng(程志海), and Shancai Wang(王善才)
Chin. Phys. B, 2023, 32 (**6**): 067103. DOI: 10.1088/1674-1056/acc7f9

Tri-hexagonal charge order in kagome metal CsV_3Sb_5 revealed by ^{121}Sb nuclear quadrupole resonance

Chao Mu(牟超), Qiangwei Yin(殷蔷薇), Zhijun Tu(涂志俊), Chunsheng Gong(龚春生), Ping Zheng(郑萍), Hechang Lei(雷和畅), Zheng Li(李政), and Jianlin Luo(雒建林)
Chin. Phys. B, 2022, 31 (**1**): 017105. DOI: 10.1088/1674-1056/ac422c

---

SPECIAL TOPIC — Recent progress on kagome metals and superconductors

Observation of a long-range unidirectional charge density wave in kagome superconductor KV_3Sb_5

Xingwei Shi(石兴伟)[1,2,†], Xiao Liu(刘潇)[1,2,†], Geng Li(李更)[1,2,3,‡], Zhen Zhao(赵振)[1,2], Haitao Yang(杨海涛)[1,2,3], Xiao Lin(林晓)[2,§], and Hong-Jun Gao(高鸿钧)[1,2,3]

[1] *School of Physical Sciences, University of Chinese Academy of Sciences, Beijing* 100190, *China*
[2] *Beijing National Center for Condensed Matter Physics and Institute of Physics, Chinese Academy of Sciences, Beijing* 100190, *China*
[3] *Hefei National Laboratory, Hefei* 230088, *China*

(Received 14 April 2025; revised manuscript received 8 May 2025; accepted manuscript online 13 May 2025)

The interplay between $2a_0 \times 2a_0$ charge density wave (CDW), nematicity and superconductivity in AV_3Sb_5 (A = K, Rb, Cs) compounds gives rise to a rich landscape of intriguing physical phenomena. In addition to the $2a_0 \times 2a_0$ CDW, a unidirectional $4a_0$ stripe CDW is also observed on the Sb surface of RbV_3Sb_5 and CsV_3Sb_5. However, reports of stripe-like CDWs in KV_3Sb_5 have been limited. Here, we report the first observation of a long-range unidirectional stripe order with a $6a_0$ modulation period on the Sb surface of KV_3Sb_5, coexisting with the $2a_0 \times 2a_0$ CDW. Notably, the intensity of the $6a_0$ stripes in STM topographies exhibits pronounced contrast reversal between opposite bias voltages. Additionally, the wave vector of the $6a_0$ modulation shows no energy-dependent dispersion, confirming its CDW origin. Furthermore, the $6a_0$ CDW is robust under a 7 T out-of-plane magnetic field and persists over a temperature range from 215 mK to 720 mK. These results provide compelling evidence for the emergence of a long-range unidirectional CDW in KV_3Sb_5.

Keywords: kagome superconductor, KV_3Sb_5, charge density wave, unidirectional strain

PACS: 71.45.Lr, 74.55.+v, 74.70.–b

DOI: 10.1088/1674-1056/add7ad **CSTR:** 32038.14.CPB.add7ad

The kagome lattice, characterized by geometric frustration and nontrivial band topology,[1,2] provides a fertile platform for exploring novel low-energy excitations in crystalline materials. Unique band structures such as flat bands,[3,4] Dirac cones[5–7] and van Hove singularities[8] emerge from the frustrated kagome network and intertwine with lattice and spin degrees of freedom in magnetic kagome systems. This interplay leads to intriguing phenomena, including the anomalous Hall effect in Mn_3Sn[9] and $Co_3Sn_2S_2$,[10] massive Dirac fermions in FeSn,[11] and correlation-driven CDW in FeGe.[12,13] In contrast to magnetic kagome materials, the discovery of the nonmagnetic kagome compound AV_3Sb_5 (A = K, Rb, Cs)[14,15] has opened new avenues for investigating and manipulating complex electronic states that arise primarily from charge degrees of freedom. In these systems, various emergent charge-ordered phases coexist and compete with superconductivity, garnering significant research attention.

Multiple symmetry-breaking charge orders have been revealed in AV_3Sb_5 compounds, including the ubiquitous in-plane $2a_0 \times 2a_0$ CDW ($T_{2a_0} \sim$ 78–104 K),[16–21] the unidirectional $4a_0$ stripe CDW in RbV_3Sb_5 and CsV_3Sb_5 ($T_{4a_0} \sim$ 55 K),[17,22–24] and charge-order-induced nematicity in CsV_3Sb_5 ($T_{\rm nem} \sim$ 35 K).[25–28] Beyond these, a $4a_0/3$ roton pair-density-wave (PDW) was initially identified in CsV_3Sb_5,[29] and more recently, a universal $2a_0 \times 2a_0$ chiral PDW has been reported across all three AV_3Sb_5 compounds,[30,31] indicating unconventional superconducting pairing and a universal rotational symmetry breaking from C_6 to C_2 within the CDW phase. Despite the close similarities in crystal structures and phase transitions among AV_3Sb_5 members, a puzzling discrepancy remains: while the robust $4a_0$ unidirectional stripe CDW has been consistently observed on the Sb-terminated surfaces of RbV_3Sb_5 and CsV_3Sb_5 via scanning tunneling microscopy/spectroscopy (STM/S), similar stripe-like features have only been sparsely reported in KV_3Sb_5,[32] and those are limited to short-range modulations. Notably, while STM experiments have directly confirmed the $4a_0$ CDW signals in RbV_3Sb_5 and CsV_3Sb_5,[17,22–25,33] this ordering remains elusive in bulk x-ray diffraction measurements across all three materials.[19,21,34] As a result, the formation mechanism of the $4a_0$ stripe CDW remains unresolved, and its apparent absence in KV_3Sb_5 is yet to be comprehensively explained.

In this paper, we present systematic STM/S measurements on the Sb-terminated surface of KV_3Sb_5 single crystal. We discover a robust unidirectional $6a_0$ stripe order within a

[†]These authors contributed equally to this work.
[‡]Corresponding author. E-mail: gengli.iop@iphy.ac.cn
[§]Corresponding author. E-mail: xlin@ucas.ac.cn

© 2025 Chinese Physical Society and IOP Publishing Ltd. All rights, including for text and data mining, AI training, and similar technologies, are reserved.

single domain, whose CDW nature is confirmed by contrast reversal in topographic images under opposite bias voltages and by the absence of energy dispersion in its wave vector. To probe its effect on the electronic structure, we performed quasiparticle interference (QPI) measurements and observed anisotropic QPI patterns originating from the V d orbitals. Moreover, the $6a_0$ order remains robust under an applied out-of-plane magnetic field of 7 T and across a temperature range of 215 mK–720 mK.

High-quality KV_3Sb_5 single crystals were synthesized using a self-flux method. STM/S measurements were carried out in a customized STM system under an ultrahigh vacuum of 1×10^{-10} mbar, with a base temperature of 4.5 K. The system was further cooled to 215 mK through ^{3}He–^{4}He dilution refrigerator. Tungsten tips, prepared by chemical etching, were annealed in ultrahigh vacuum to remove surface oxides and adsorbed contaminants, and subsequently calibrated on a clean Au(111) surface prior to use. To suppress the diffusion of exposed K atoms, the KV_3Sb_5 crystals were mechanically cleaved at approximately 12 K in an ultrahigh vacuum environment and immediately transferred to the STM scanner, yielding clean and extended Sb-terminated surfaces. Differential conductance maps, $\mathrm{d}I/\mathrm{d}V(r,V)$, were acquired using a standard lock-in technique at a frequency of 931.77 Hz with an excitation voltage of 0.02 mV.

KV_3Sb_5 crystallizes in the space group $P6/mmm$ (No. 191) in its normal state. It features a typical layered structure composed of alternating K–Sb_2–VSb_1–Sb_2–K stacking layers (Fig. 1(a)). The VSb_1 slab consists of a V-based kagome network interwoven with a hexagonal Sb_1 lattice. K atoms are positioned directly above Sb_1 atoms along the c-axis, while Sb_2 atoms reside above the center of the corner-sharing triangles in the V-based kagome lattice, forming a honeycomb arrangement. Due to weak interlayer coupling, KV_3Sb_5 crystals can be readily cleaved between the Sb_2 and K layers, typically exposing either Sb- or K-terminated surfaces. On the Sb-terminated surface, a $2a_0 \times 2a_0$ CDW is commonly observed (Fig. 1(b)). However, in a KV_3Sb_5 sample cleaved under low temperature ($\sim$ 12 K), we observe a new type of periodic stripe modulation, as highlighted by the yellow dashed lines (Fig. 1(c)). These stripes are aligned along one crystallographic direction, with a spacing of six times the lattice constant, indicating a unidirectional $6a_0$ modulation.

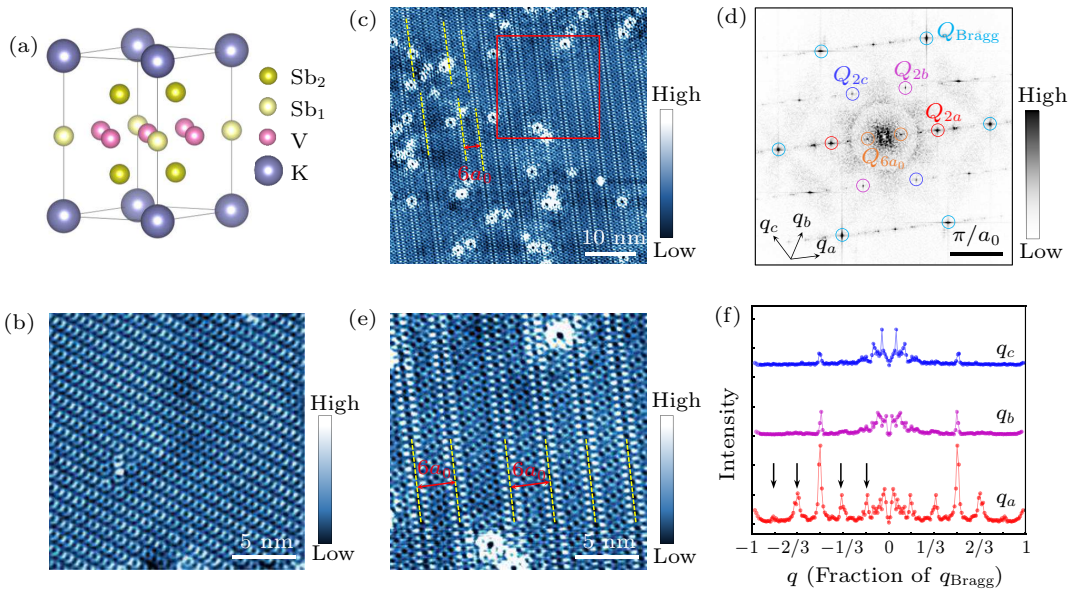


Fig. 1. The crystal structure and STM topography of the Sb surface of KV_3Sb_5. (a) Atomic models of the crystalline structure of KV_3Sb_5. (b) A typical STM topography of a Sb-terminated surface, showing the $2a_0 \times 2a_0$ CDW pattern. (c) A 50 nm×50 nm STM topography, showing the presence of uniaxial stripes. (d) FT image of (b), showing the coexistence of the $6a_0$ and the $2a_0 \times 2a_0$ orders. The cyan circles label the Q_{Bragg} peaks. The $2a_0 \times 2a_0$ CDW peaks of Q_{2a}, Q_{2b} and Q_{2c} are highlighted by red, purple and blue circles. The $6a_0$ peaks Q_{6a_0} are outlined by the orange circles. (e) Atomically-resolved STM image of the red square in (c). The $2a_0 \times 2a_0$ CDW and unidirectional $6a_0$ stripe-like modulations are both clearly resolved, with stripes highlighted by yellow dashed lines. (f) FT linecuts along $\boldsymbol{q}_a$, $\boldsymbol{q}_b$ and $\boldsymbol{q}_c$ in (d). Scanning conditions in (b), (c) and (e): $V_{\mathrm{sample}} = -10$ mV, $I_{\mathrm{set}} = 100$ pA.

These periodic stripe modulations are reminiscent of the unidirectional $4a_0$ stripe CDW previously observed in RbV_3Sb_5 and CsV_3Sb_5. Fourier transform (FT) analysis (Fig. 1(d)) reveals distinct wave vector peaks corresponding to the stripe order (Q_{6a_0}), highlighted by orange circles. In comparison, lattice-related Bragg peaks (Q_{Bragg}) are marked with cyan circles, while the FT peaks associated with the $2a_0 \times 2a_0$ CDW are denoted by red (Q_{2a}), purple (Q_{2b}) and blue (Q_{2c}) circles. By examining intensity profiles along the three high-symmetry directions ($\boldsymbol{q}_a$, $\boldsymbol{q}_b$ and $\boldsymbol{q}_c$) and plotting the corresponding line cuts in Fig. 1(f), we observe that both the fundamental and higher-order wave vector peaks associated with the stripe order appear exclusively along the $\boldsymbol{q}_a$ direction. These peaks are precisely located at integral multiples

of $\pm 1/6$ of q_{Bragg}, indicating a real-space modulation period of $6a_0$ — consistent with the uniform $6a_0$ spacing between adjacent stripes observed in the topographic image. Additionally, occurrences of spacing larger than $6a_0$ between stripes are occasionally observed (Fig. 1(e)), likely resulting from dislocations between two adjacent $6a_0$ stripes, as indicated by yellow dashed lines (Fig. 1(c)). Based on these findings, the observed superlattice is defined as a unidirectional $6a_0$ stripe order (Q_{6a_0}). The discovery of Q_{6a_0} CDW marks the first observation of a long-range unidirectional stripe order in KV_3Sb_5, filling the previously noted gap in the AV_3Sb_5 family.

To investigate the electronic properties of the $6a_0$ stripe order, bias-dependent STM topographies were acquired at 420 mK in a different region exhibiting clear $6a_0$ stripe modulation. The tunneling current (I_{set}) was fixed at 100 pA, while the sample bias voltage was varied from -100 mV to $+100$ mV. Across this wide energy range, the $6a_0$ stripe order remains clearly visible in the topographies (Figs. 2(a)–2(f)). The randomly distributed dark spots present in the images are attributed to Sb vacancies located within the VSb_1 slab. These defects exhibit nearly constant contrast regardless of the applied bias voltage, thereby serving as convenient reference markers to track the relative position of the unidirectional stripes. As indicated by yellow dashed lines (Figs. 2(a) and 2(d)), a stripe appearing dark at negative bias voltage becomes bright at positive bias, demonstrating a pronounced contrast reversal. Similar bias-dependent contrast phenomena have been reported in other CDW systems,[35,36] and are recognized as an indication of charge density wave formation. This behavior closely resembles that of the $4a_0$ CDW in RbV_3Sb_5 and CsV_3Sb_5, reinforcing the conclusion that the $6a_0$ stripe order in KV_3Sb_5 possesses CDW characteristics.

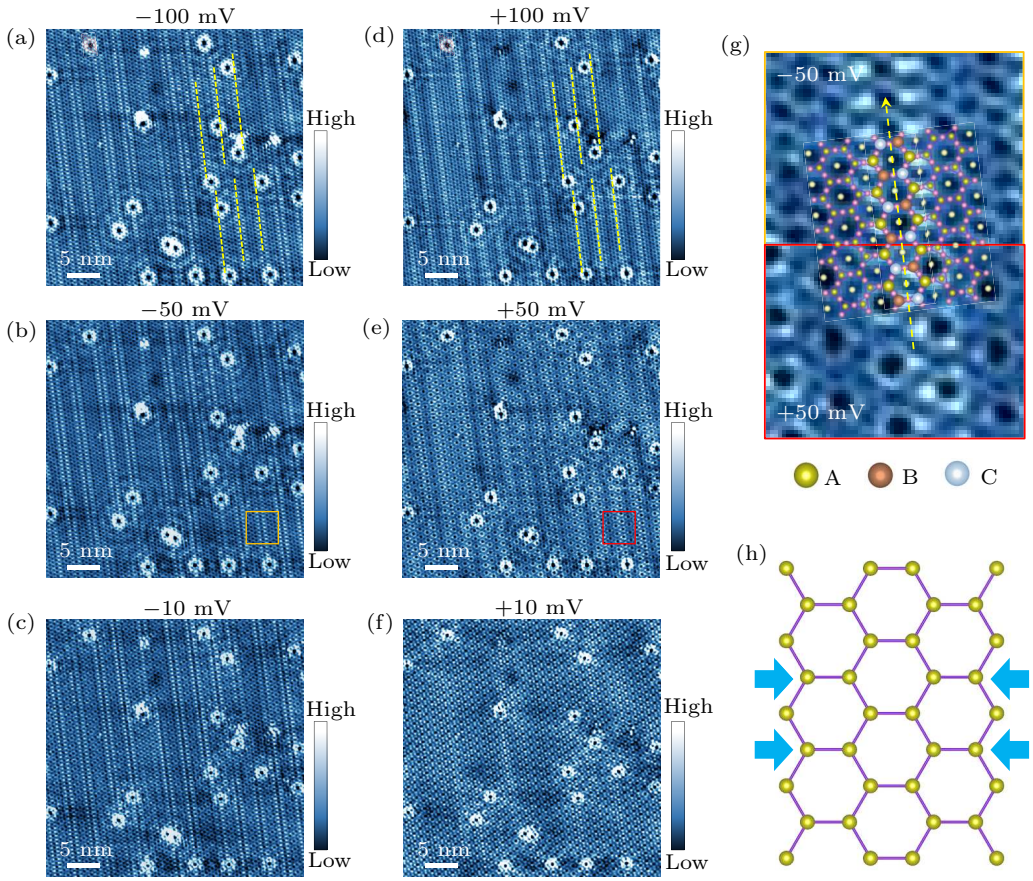


Fig. 2. Contrast reversal of the stripe features under the positive and the negative bias voltages. (a)–(f) STM topographies of the same region under bias voltages of -100 mV, -50 mV, -10 mV, 10 mV, 50 mV, and 100 mV, respectively, showing stable $6a_0$ stripe modulation. (g) Zoom-in STM image of the solid squares in (b) (upper panel) and (e) (lower panel). Different Sb atoms are highlighted as A (yellow), B (brown), C (silver). (h) Schematic of uniaxial strain applied to the atomic plane. The tunneling current is fixed at $I_{\mathrm{set}} = 100$ pA for (a)–(g).

More intriguingly, within a single Sb honeycomb unit cell along the $6a_0$ stripe, we observe three nonequivalent Sb sites (labeled A, B, and C) that exhibit distinct intensity changes under opposite bias voltages (Fig. 2(g)). In contrast, Sb atoms far from the stripe center show less variation. At -50 mV, the strongest intensity appears close to the A sites, whereas at $+50$ mV, it shifts between the B and C sites — closer to the stripe center. This redistribution of local density of states among different Sb sites under opposite bias voltages is directly responsible for the observed contrast reversal. A plausible explanation for this effect involves local strain in the atomic planes, potentially induced by low-temperature cleavage, as schematically illustrated in Fig. 2(h). This strain-driven lattice distortion may play a key role in stabilizing the unidi-

rectional CDW order on the Sb surface of KV_3Sb_5. RbV_3Sb_5 and CsV_3Sb_5 have larger lattice constants and radii of alkali atoms compared to KV_3Sb_5, which results in lower structural stability and enhanced susceptibility to external perturbations. This makes them more prone to structural phase transitions under external pressure and temperature variations.[37,38] Forming a long-range stripe CDW in the stable KV_3Sb_5 crystal is challenging, as the local strain must exceed a critical threshold to induce appropriate periodic lattice distortions. As a result, stripe CDW is generally observed in RbV_3Sb_5 and CsV_3Sb_5 but is rare in KV_3Sb_5. Additionally, the local strain on the surface is inhomogeneous, meaning that stripe CDW can only be observed in certain regions. This is similar to previous studies on strain-induced stripe CDW in $NbSe_2$.[39,40]

We further carried out quasiparticle interference (QPI) measurements in the same region. The real-space $6a_0$ stripe order exhibits clear contrast reversal under opposite bias voltages, consistent with the bias-dependent topographies described earlier (Figs. 3(a) and 3(b)). Notably, the corresponding wave vector associated with the $6a_0$ modulation (Q_{6a_0}) exhibits no discernible energy dispersion within the energy range of ± 5 mV (Fig. 3(c)). This non-dispersive behavior provides additional strong evidence that the $6a_0$ stripe modulation arises from a static charge order, further confirming its identity as an unidirectional charge density wave (CDW).[16]

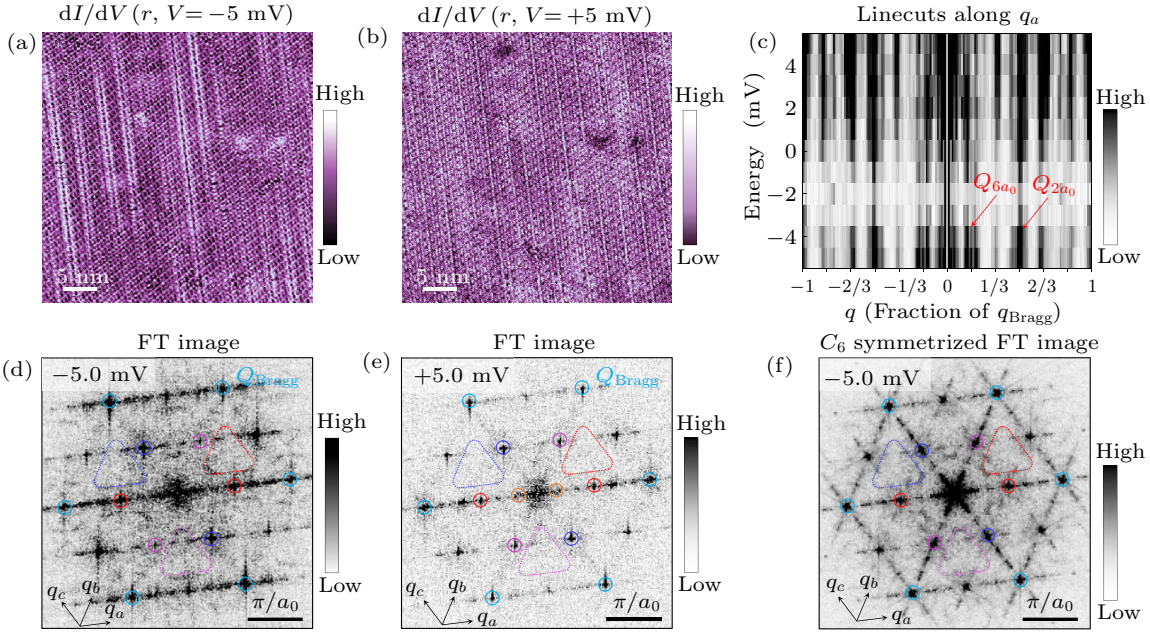


Fig. 3. Energy dependence of the stripe order. (a) and (b) Typical $dI/dV(r,V)$ maps at -5 mV and $+5$ mV, showing the $6a_0$ stripe modulation. (c) Intensity plot of the FT linecuts along $\boldsymbol{q}_a$ under different energies. The $6a_0$ stripe order shows no energy dispersion. (d) and (e) The FT images of (a) and (b), respectively. (f) C_6 symmetrized FT image of (d). The three triangular contours represent the quasiparticle interference pattern. Setup conditions for maps: $V_{sample} = -5$ mV, $I_{set} = 1$ nA.

To probe the band structure of KV_3Sb_5 in the presence of the $6a_0$ CDW, we analyzed the coherent QPI patterns extracted from the FT images of the differential conductance maps, $dI/dV(r,V)$. Three sets of triangular QPI patterns are clearly resolved (Figs. 3(d) and 3(e)). To enhance the signal-to-noise ratio, the FT shown in Fig. 3(d) has been symmetrized with a C_6 rotation operation and is displayed in Fig. 3(f). In line with previous studies,[22,25,30,33] these triangular QPI features originate from intra-valley scattering processes of electrons from the V d orbitals. The triangles show varying intensities along different directions, suggesting a rotational symmetry breaking from C_6 to C_2, which is indicative of electronic nematicity.

Interestingly, we do not observe the one-dimensional QPI feature (q_{1D}), which has previously been detected only in CsV_3Sb_5 hosting a unidirectional $4a_0$ CDW.[22,25,29,33] The q_{1D} pattern, generally interpreted as a fingerprint of charge nematicity, is known to align with the direction of the stripe CDW in CsV_3Sb_5. However, temperature-dependent QPI measurements have shown that q_{1D} and the $4a_0$ CDW possess different onset temperatures,[22] implying that the unidirectional stripe CDW is not the primary driver of nematicity in CsV_3Sb_5. The absence of q_{1D} in KV_3Sb_5, despite the presence of unidirectional $6a_0$ CDW, provides further evidence supporting this conclusion. These observations suggest that the rotational symmetry breaking observed in the QPI patterns is unrelated to the unidirectional stripe CDW, and is instead likely linked to the intrinsic formation of the $2a_0 \times 2a_0$ chiral CDW phase.

We then performed temperature- and magnetic-field-dependent investigations of the $6a_0$ stripe CDW. In a continuous temperature-dependent STM measurement from 215 mK to 720 mK, the $6a_0$ stripe modulation remains clearly visible in topographies (Figs. 4(a)–4(f)) without any discernible

changes in the topography. FT linecuts along the $\boldsymbol{q}_a$ direction confirm that the $6a_0$ stripe CDW is robust, exhibiting no energy dispersion under either out-of-plane magnetic field (7 T) or varying temperature (Fig. 4(i)). It is noteworthy that the first-order peak of the $6a_0$ stripe order appears near the center of the low-frequency region in the FT, resulting in a relatively weak signal. However, the higher-order peaks, highlighted by orange dashed lines, are clearly observed at 1/3 and 2/3 times of q_{Bragg}, with negligible deviation due to slight dislocations between neighboring stripes (Fig. 4(i)). These findings further support the intrinsic robustness of the $6a_0$ stripe CDW in KV_3Sb_5.

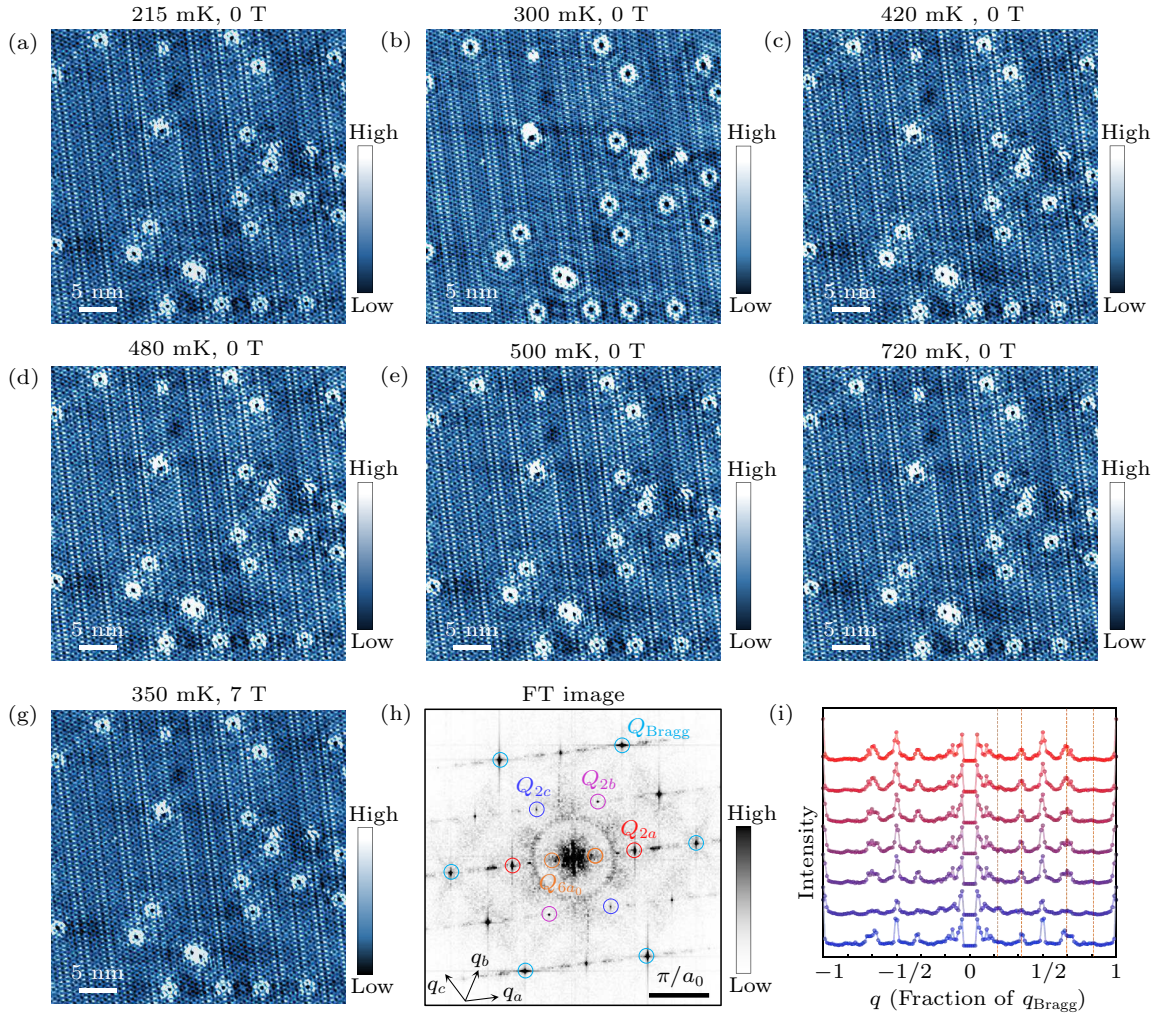


Fig. 4. Temperature and magnetic field dependence of the $6a_0$ stripe CDW. (a)–(f) Temperature dependent STM topographies taken from 215 mK to 720 mK. (g) STM topography of the $6a_0$ stripe taken under a vertical magnetic field of 7 T. (h) FT image of (g) showing clear $6a_0$ spot along $\boldsymbol{q}_a$. (i) Waterfall plot of FT linecuts along $\boldsymbol{q}_a$ under different temperatures and magnetic fields. From bottom to top, the experimental conditions are 215 mK, 300 mK, 350 mK with 7 T field, 420 mK, 480 mK, 520 mK and 720 mK, respectively. The $6a_0$ stripe CDW vector peaks and its related high-order peak signals are indicated by orange dashed lines in (i). Setup conditions: (b) $V_{\text{sample}} = -100$ mV, $I_{\text{set}} = 100$ pA; (a) and (c)–(g) $V_{\text{sample}} = -10$ mV, $I_{\text{set}} = 100$ pA.

In summary, we have used STM to uncover a uniform long-range stripe order with a $6a_0$ modulation period on the Sb-terminated surface of KV_3Sb_5. This commensurate $6a_0$ stripe order is identified as a unidirectional charge density wave, based on characteristic contrast reversal under opposite bias voltages and the absence of energy dispersion. The stripe CDW remains stable under a 7 T out-of-plane magnetic field and is found to persist across a broad temperature range. We propose that this stripe CDW likely originates from strain-induced lattice distortions of the Sb surface. Our findings highlight the need for further theoretical and experimental studies to fully understand the emergence of stripe CDWs in AV_3Sb_5 compounds and their potential interplay with the $2a_0 \times 2a_0$ chiral CDW, electronic nematicity, and superconductivity.

Acknowledgements

Project supported by the National Key Research and Development Project of China (Grant Nos. 2024YFA1207700 and 2022YFA1204100), the National Natural Science Foundation of China (Grant No. 62488201), the CAS Project for Young Scientists in Basic Research (Grant No. YSBR-003), the Youth Innovation Promotion Association (Grant No. 2023005), and the Innovation Program of Quantum Sci-

ence and Technology (Grant No. 2021ZD0302700).

References

[1] Kiesel M L and Thomale R 2012 *Phys. Rev. B* **86** 121105
[2] Wang W S, Li Z Z, Xiang Y Y and Wang Q H 2013 *Phys. Rev. B* **87** 115135
[3] Kang M, Fang S, Ye L, Po H C, Denlinger J, Jozwiak C, Bostwick A, Rotenberg E, Kaxiras E, Checkelsky J G and Comin R 2020 *Nat. Commun.* **11** 4004
[4] Riberolles S X M, Slade T J, Han T, Li B, Abernathy D L, Canfield P C, Ueland B G, Orth P P, Ke L and McQueeney R J 2024 *Nat. Commun.* **15** 1592
[5] Liu Z, Li M, Wang Q, Wang G, Wen C, Jiang K, Lu X, Yan S, Huang Y, Shen D, Yin J X, Wang Z, Yin Z, Lei H and Wang S 2020 *Nat. Commun.* **11** 4002
[6] Zhang T, Yilmaz T, Vescovo E, Li H X, Moore R G, Lee H N, Miao H, Murakami S and McGuire M A 2022 *npj Comput. Mater.* **8** 1
[7] Shi M, Yu F, Yang Y, Meng F, Lei B, Luo Y, Sun Z, He J, Wang R, Jiang Z, Liu Z, Shen D, Wu T, Wang Z, Xiang Z, Ying J and Chen X 2022 *Nat. Commun.* **13** 2773
[8] Kiesel M L, Platt C and Thomale R 2013 *Phys. Rev. Lett.* **110** 126405
[9] Nakatsuji S, Kiyohara N and Higo T 2015 *Nature* **527** 212
[10] Liu E, Sun Y, Kumar N, Muechler L, Sun A, Jiao L, Yang S Y, Liu D, Liang A, Xu Q, Kroder J, Süß V, Borrmann H, Shekhar C, Wang Z, Xi C, Wang W, Schnelle W, Wirth S, Chen Y, Goennenwein S T B and Felser C 2018 *Nat. Phys.* **14** 1125
[11] Ye L, Kang M, Liu J, von Cube F, Wicker C R, Suzuki T, Jozwiak C, Bostwick A, Rotenberg E, Bell D C, Fu L, Comin R and Checkelsky J G 2018 *Nature* **555** 638
[12] Wu L, Hu Y, Fan D, Wang D and Wan X 2023 *Chin. Phys. Lett.* **40** 117103
[13] Teng X, Oh J S, Tan H, Chen L, Huang J, Gao B, Yin J X, Chu J H, Hashimoto M, Lu D, Jozwiak C, Bostwick A, Rotenberg E, Granroth G E, Yan B, Birgeneau R J, Dai P and Yi M 2023 *Nat. Phys.* **19** 814
[14] Ortiz B R, Gomes L C, Morey J R, Winiarski M, Bordelon M, Mangum J S, Oswald I W H, Rodriguez-Rivera J A, Neilson J R, Wilson S D, Ertekin E, McQueen T M and Toberer E S 2019 *Phys. Rev. Mater.* **3** 094407
[15] Ortiz B R, Teicher S M L, Hu Y, Zuo J L, Sarte P M, Schueller E C, Abeykoon A M M, Krogstad M J, Rosenkranz S, Osborn R, Seshadri R, Balents L, He J and Wilson S D 2020 *Phys. Rev. Lett.* **125** 247002
[16] Jiang Y X, Yin J X, Denner M M, Shumiya N, Ortiz B R, Xu G, Guguchia Z, He J, Hossain M S, Liu X, Ruff J, Kautzsch L, Zhang S S, Chang G, Belopolski I, Zhang Q, Cochran T A, Multer D, Litskevich M, Cheng Z J, Yang X P, Wang Z, Thomale R, Neupert T, Wilson S D and Hasan M Z 2021 *Nat. Mater.* **20** 1353
[17] Shumiya N, Hossain Md S, Yin J X, Jiang Y X, Ortiz B R, Liu H, Shi Y, Yin Q, Lei H, Zhang S S, Chang G, Zhang Q, Cochran T A, Multer D, Litskevich M, Cheng Z J, Yang X P, Guguchia Z, Wilson S D and Hasan M Z 2021 *Phys. Rev. B* **104** 35131
[18] Luo J, Zhao Z, Zhou Y Z, Yang J, Fang A F, Yang H T, Gao H J, Zhou R and Zheng G Q 2022 *npj Quantum Mater.* **7** 1
[19] Li H, Zhang T T, Yilmaz T, Pai Y Y, Marvinney C E, Said A, Yin Q W, Gong C S, Tu Z J, Vescovo E, Nelson C S, Moore R G, Murakami S, Lei H C, Lee H N, Lawrie B J and Miao H 2021 *Phys. Rev. X* **11** 031050
[20] Li H, Zhao H, Ortiz B R, Park T, Ye M, Balents L, Wang Z, Wilson S D and Zeljkovic I 2022 *Nat. Phys.* **18** 265
[21] Li H, Fabbris G, Said A H, Sun J P, Jiang Y X, Yin J X, Pai Y Y, Yoon S, Lupini A R, Nelson C S, Yin Q W, Gong C S, Tu Z J, Lei H C, Cheng J G, Hasan M Z, Wang Z, Yan B, Thomale R, Lee H N and Miao H 2022 *Nat. Commun.* **13** 6348
[22] Zhao H, Li H, Ortiz B R, Teicher S M L, Park T, Ye M, Wang Z, Balents L, Wilson S D and Zeljkovic I 2021 *Nature* **599** 216
[23] Hu B, Ye Y, Huang Z, Han X, Zhao Z, Yang H, Chen H and Gao H J 2022 *Chin. Phys. B* **31** 058102
[24] Wang Z, Jiang Y X, Yin J X, Li Y, Wang G Y, Huang H L, Shao S, Liu J, Zhu P, Shumiya N, Hossain M S, Liu H, Shi Y, Duan J, Li X, Chang G, Dai P, Ye Z, Xu G, Wang Y, Zheng H, Jia J, Hasan M Z and Yao Y 2021 *Phys. Rev. B* **104** 75148
[25] Wu P, Tu Y, Wang Z, Yu S, Li H, Ma W, Liang Z, Zhang Y, Zhang X, Li Z, Yang Y, Qiao Z, Ying J, Wu T, Shan L, Xiang Z, Wang Z and Chen X 2023 *Nat. Phys.* **19** 1143
[26] Nie L, Sun K, Ma W, Song D, Zheng L, Liang Z, Wu P, Yu F, Li J, Shan M, Zhao D, Li S, Kang B, Wu Z, Zhou Y, Liu K, Xiang Z, Ying J, Wang Z, Wu T and Chen X 2022 *Nature* **604** 59
[27] Xu Y, Ni Z, Liu Y, Ortiz B R, Deng Q, Wilson S D, Yan B, Balents L and Wu L 2022 *Nat. Phys.* **18** 1470
[28] Fukushima K, Obata K, Yamane S, Hu Y, Li Y, Yao Y, Wang Z, Maeno Y and Yonezawa S 2024 *Nat. Commun.* **15** 2888
[29] Chen H, Yang H, Hu B, Zhao Z, Yuan J, Xing Y, Qian G, Huang Z, Li G, Ye Y, Ma S, Ni S, Zhang H, Yin Q, Gong C, Tu Z, Lei H, Tan H, Zhou S, Shen C, Dong X, Yan B, Wang Z and Gao H J 2021 *Nature* **599** 222
[30] Deng H, Qin H, Liu G, Yang T, Fu R, Zhang Z, Wu X, Wang Z, Shi Y, Liu J, Liu H, Yan X Y, Song W, Xu X, Zhao Y, Yi M, Xu G, Hohmann H, Holbæk S C, Dürrnagel M, Zhou S, Chang G, Yao Y, Wang Q, Guguchia Z, Neupert T, Thomale R, Fischer M H and Yin J X 2024 *Nature* **632** 775
[31] Yan X Y, Deng H, Yang T, Liu G, Song W, Miao H, Tu Z, Lei H, Wang S, Lin B C, Qin H and Yin J X 2024 *Chin. Phys. Lett.* **41** 97401
[32] Li H, Oh D, Kang M, Zhao H, Ortiz B R, Oey Y, Fang S, Ren Z, Jozwiak C, Bostwick A, Rotenberg E, Checkelsky J G, Wang Z, Wilson S D, Comin R and Zeljkovic I 2023 *Phys. Rev. X* **13** 031030
[33] Li H, Zhao H, Ortiz B R, Oey Y, Wang Z, Wilson S D and Zeljkovic I 2023 *Nat. Phys.* **19** 637
[34] Xiao Q, Lin Y, Li Q, Zheng X, Francoual S, Plueckthun C, Xia W, Qiu Q, Zhang S, Guo Y, Feng J and Peng Y 2023 *Phys. Rev. Res.* **5** L012032
[35] Arguello C J, Chockalingam S P, Rosenthal E P, Zhao L, Gutiérrez C, Kang J H, Chung W C, Fernandes R M, Jia S, Millis A J, Cava R J and Pasupathy A N 2014 *Phys. Rev. B* **89** 235115
[36] Fang A, Ru N, Fisher I R and Kapitulnik A 2007 *Phys. Rev. Lett.* **99** 46401
[37] Tan H, Liu Y, Wang Z and Yan B 2021 *Phys. Rev. Lett.* **127** 46401
[38] Zheng L, Wu Z, Yang Y, Nie L, Shan M, Sun K, Song D, Yu F, Li J, Zhao D, Li S, Kang B, Zhou Y, Liu K, Xiang Z, Ying J, Wang Z, Wu T and Chen X 2022 *Nature* **611** 682
[39] Soumyanarayanan A, Yee M M, He Y, van Wezel J, Rahn D J, Rossnagel K, Hudson E W, Norman M R and Hoffman J E 2013 *Proc. Natl. Acad. Sci. USA* **110** 1623
[40] Gao S, Flicker F, Sankar R, Zhao H, Ren Z, Rachmilowitz B, Balachandar S, Chou F, Burch K S, Wang Z, van Wezel J and Zeljkovic I 2018 *Proc. Natl. Acad. Sci. USA* **115** 6986